



# CHORUS

This is the accepted manuscript made available via CHORUS. The article has been published as:

## Isostable reduction of periodic orbits

Dan Wilson and Jeff Moehlis

Phys. Rev. E **94**, 052213 — Published 14 November 2016

DOI: [10.1103/PhysRevE.94.052213](https://doi.org/10.1103/PhysRevE.94.052213)

# Isostable Reduction of Periodic Orbits

Dan Wilson and Jeff Moehlis

*Department of Mechanical Engineering, University of California, Santa Barbara, CA 93106, USA*

The well-established method of phase reduction neglects information about a limit cycle oscillator's approach towards its periodic orbit. Consequently, phase reduction suffers in practicality unless the magnitude of the Floquet multipliers of the underlying limit cycle are small in magnitude. By defining isostable coordinates of a periodic orbit, we present an augmentation to classical phase reduction which obviates this restriction on the Floquet multipliers. This framework allows for the study and understanding of periodic dynamics for which standard phase reduction alone is inadequate. Most notably, isostable reduction allows for a convenient and self-contained characterization of the dynamics near unstable periodic orbits.

PACS numbers: 02.30.Mv, 02.30.Hq, 05.45.Gg, 87.10.Ca

Oscillatory behavior is a ubiquitous natural phenomenon with a wide array of applications including neurological behavior, circadian rhythms, chemical reactions, mechanical vibrations, and chaotic systems [1–7]. For nearly half a century, phase reduction has been an indispensable tool to aid in the understanding and manipulation of such oscillators [1–6] by allowing periodic solutions of

$$\dot{\mathbf{x}} = F(\mathbf{x}) + G(\mathbf{x}, t), \quad \mathbf{x} \in \mathbb{R}^n \quad (1)$$

to be represented by the single variable system:

$$\dot{\theta} = \omega + Q(\theta)^T G(\mathbf{x}, t). \quad (2)$$

Here,  $G \in \mathbb{R}^n$  is an external perturbation,  $\theta \in [0, 2\pi)$  is the phase of oscillation,  $\omega = 2\pi/T$  is the natural frequency with  $T$  being the natural period, and  $Q(\theta) \in \mathbb{R}^n$  is an infinitesimal phase response curve (PRC), which as its name suggests, is valid for perturbations  $G$  with small magnitude. Practically, (2) is valid in a close vicinity of the periodic orbit,  $\gamma$ . Consequently, the amplitude of allowable perturbations is limited by the size of the Floquet multipliers [8]; stable orbits with Floquet multipliers with magnitude close to 1 can only admit relatively small perturbations without the risk of being driven away from the limit cycle over time. In many applications [5, 9–11], however, the efficacy of a given control strategy is directly related to the magnitude of allowable perturbations. Furthermore, for unstable periodic orbits, (2) alone cannot adequately describe the long term behavior of (1), rendering it unusable. Discrete time proportional state feedback [7, 12] and delayed feedback control [13] has been used to suppress chaos by means of stabilizing unstable periodic orbits. These classes of chaos control strategies have found practical applications in cardiac, electronic, networked and optical systems [14–17]. Phase reduction techniques could be of practical interest in the suppression of chaos if appropriate modifications could be made.

This work proposes an augmentation of standard phase reduction which allows for a better understanding of systems with either a stable or unstable periodic orbit. We introduce a set of isostable coordinates and associated isostable response curves (IRCs), which represent the distance from the periodic orbit in an appropriate basis. The notion of isostables was introduced in [18] (c.f. [19] and [20]) to represent sets of initial conditions which converge toward a stable fixed point together, in a well-defined sense. The isostable coordinates used in this manuscript are defined in a manner that is similar in spirit, but adapted for use with periodic orbits. Unlike [21, 22], the strategy proposed here does not require computationally intensive calculations of an *ad hoc* coordinate system with respect to a periodic orbit of dimensionality greater than 2. Furthermore, the strategy presented here does not require the periodic orbit to be exponentially attracting in either forward or backward time. In the examples given in this work, we illustrate the utility of this reduction method in two different oscillatory systems for which (2) alone is insufficient.

Starting with a general system of ordinary differential equations (1), let  $\gamma$  be  $T$ -periodic orbit which exists for  $G \equiv 0$ . We define a scalar phase variable on  $\gamma$  such that  $\theta(\mathbf{x}) : \mathbb{R}^n \rightarrow [0, 2\pi)$  for which  $d\theta(\mathbf{x}(t))/dt = \omega$  and  $\theta(\mathbf{x}(t)) = \theta(\mathbf{x}(t + T))$ , and choose an arbitrary point  $\mathbf{x}_0 \in \gamma$  for which  $\theta(\mathbf{x}_0) = 0$ . By solving for  $Q(\theta)$  (the gradient of the phase field) using, e.g., adjoint methods [4, 23, 24], this notion of phase can be extended to any  $\mathbf{x}$  in a neighborhood of  $\gamma$  by noting that for  $\epsilon > 0$ ,  $\theta(\mathbf{x} + \epsilon\mathbf{y}) = \theta(\mathbf{x}) + \mathcal{O}(\epsilon^2)$  for any  $\mathbf{y}$  in the null space of  $Q(\theta(\mathbf{x}))$ . This definition of phase is possible regardless of the stability type of  $\gamma$ . We define isochrons as level sets of the phase field, i.e.  $\Gamma_\theta = \{\mathbf{x} | \theta(\mathbf{x}) = \theta\}$ . When  $\gamma$  is a stable periodic orbit, isochrons have an intuitive meaning: for any initial conditions  $\mathbf{a}(0) \in \gamma$  and  $\mathbf{b}(0)$  in the basin of attraction of  $\gamma$  on the same isochron,  $\lim_{t \rightarrow \infty} \|\mathbf{a}(t) - \mathbf{b}(t)\| = 0$  [1].

Changing to phase variables using the chain rule, one arrives at the phase reduction (2). Here, we are also interested in the transient behavior of (1) near  $\gamma$  which can be understood in terms of Poincaré maps. By construction, any initial condition in  $\Gamma_0$  first returns to  $\Gamma_0$  at time  $T$  allowing for the definition of a Poincaré map,

$$P : \Gamma_0 \rightarrow \Gamma_0; \quad \mathbf{x} \mapsto \phi(\mathbf{x}), \quad (3)$$

with  $P(\mathbf{x}_0) = \mathbf{x}_0$ . In a small neighborhood of  $\mathbf{x}_0$  we may approximate  $\phi$  from (3) as

$$\phi(\mathbf{x}) = \mathbf{x}_0 + J_P(\mathbf{x} - \mathbf{x}_0) + \mathcal{O}(\|\mathbf{x} - \mathbf{x}_0\|^2), \quad (4)$$

where  $J_P = d\phi/d\mathbf{x}|_{\mathbf{x}_0}$ . Suppose  $J_P$  is diagonalizable and let  $V \in \mathbb{R}^{n \times n}$  be a matrix with columns that form an basis of unit length eigenvectors  $\{\mathbf{v}_k, k = 1, \dots, n\}$  of  $J_P$  with associated eigenvalues  $\{\lambda_k, k = 1, \dots, n\}$ . The eigenvalues  $\lambda_i$  are often referred to as Floquet multipliers of the periodic orbit. For any eigenvector  $v_i$  with associated  $\lambda_i \in \mathbb{R} > 0$  (if any  $\lambda_i < 0$ , one can define the period to be  $2T$  so that all eigenvalues are positive), we can define a set of isostable coordinates,

$$\psi_i(\mathbf{x}) = \mathbf{e}_i^T V^{-1}(\mathbf{x}_\Gamma - \mathbf{x}_0) \exp(-\log(\lambda_i)t_\Gamma/T). \quad (5)$$

Here,  $\mathbf{x}_\Gamma$  and  $t_\Gamma \in [0, T)$  are defined to be the location and time, respectively, at which the trajectory first returns to  $\Gamma_0$  under the flow  $\dot{\mathbf{x}} = F(\mathbf{x})$  and  $\mathbf{e}_i$  is a vector with 1 in the  $i^{\text{th}}$  position and zeros elsewhere. These isostable coordinates  $\psi_i(\mathbf{x})$  are defined for all  $\mathbf{x} \in \mathbb{R}^n$ , not just on the Poincaré section. Intuitively, a trajectory near the periodic orbit will spiral towards or away at a rate determined by each of the Floquet multipliers. This growth/decay is matched by the decay/growth of the exponential term from (5), giving a sense of the distance in directions transverse to the periodic orbit. Noting that  $dt_\Gamma/dt = -1$  for  $\mathbf{x}(t) \notin \Gamma_0$ , by direct differentiation of (5)  $d\psi_i/dt = \psi_i \log(\lambda_i)/T$ , therefore,

$$\nabla \psi_i(\mathbf{x}) \cdot F(\mathbf{x}) = \psi_i \log(\lambda_i)/T. \quad (6)$$

By (4), one can verify that under the flow  $\dot{\mathbf{x}} = F(\mathbf{x})$ ,  $\psi_i(\mathbf{x}(t_\Gamma^+)) = \psi_i(\mathbf{x}(t_\Gamma^-)) + \mathcal{O}(\|\mathbf{x} - \mathbf{x}_0\|^2)$ . This discontinuity results from the approximation of (3) as a linear mapping. Throughout this analysis, we will assume close enough proximity to the periodic orbit so that this discontinuity is negligible. Figure 1 gives a representation of a general 2-dimensional system in terms of its isostable coordinates. For an arbitrary time  $\tau$ , if we compute the isostable coordinate  $\psi(\mathbf{x}(\tau)) = \vartheta$ , after one revolution,  $\psi(\mathbf{x}(\tau + T)) = \lambda_1 \vartheta + \mathcal{O}(\|\mathbf{x} - \mathbf{x}_0\|^2)$ . Furthermore, close to the periodic orbit, when the Poincaré map (3) is well approximated by a linear mapping, two initial conditions

on the same isostable level set will cross successive isostable level sets together on their way to the limit cycle (to leading order)

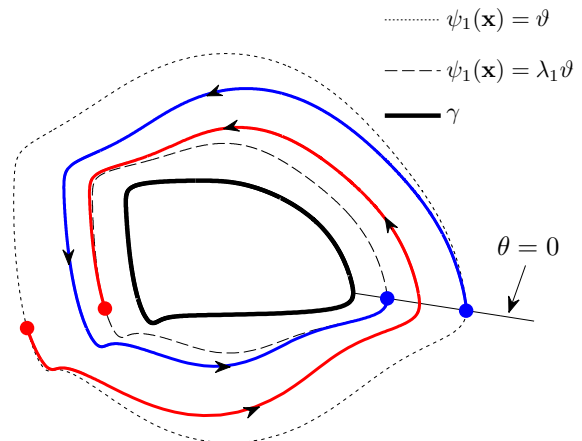


FIG. 1. A sketch of the behavior of a general 2-dimensional system near its limit cycle. The red and blue lines represent two trajectories integrated over one period which start on the same isostable level set. Dashed and dotted lines represent two different isostable level sets. When the Poincaré map defined with respect to the  $\theta = 0$  isochron is well approximated as a linear map the discontinuity across the  $\theta = 0$  isochron is negligible, and trajectories on the same isostable level set cross the successive isostable level sets together. Furthermore, the isostable coordinate decreases at an exponential rate governed by the Floquet multiplier  $\lambda_1$ . Here, isostable level sets give a sense of the distance from the periodic orbit.

Letting  $\kappa_i \equiv \log(\lambda_i)/T$ , and changing variables to isostable coordinates, with the chain rule we find

$$\begin{aligned} \frac{d\psi_i(\mathbf{x})}{dt} &= \nabla \psi_i(\mathbf{x}) \cdot (F(\mathbf{x}) + G(\mathbf{x}, t)) \\ &= \kappa_i \psi_i(\mathbf{x}) + \nabla \psi_i(\mathbf{x}) \cdot G(\mathbf{x}, t). \end{aligned} \quad (7)$$

Evaluating the vector field at  $\mathbf{x}^\gamma(\theta, \psi_i)$ , which we define as the intersection of the trajectory  $\gamma$ , the  $\psi_i(\mathbf{x})$  level set (i.e. isostable), and the  $\theta(\mathbf{x})$  level set (i.e. isochron), we have

$$\frac{d\psi_i(\mathbf{x})}{dt} = \kappa_i \psi_i(\mathbf{x}) + \nabla \psi_i(\mathbf{x}^\gamma(\theta, \psi_i)) \cdot G(\mathbf{x}^\gamma(\theta, \psi_i), t). \quad (8)$$

Here, as in [25] we have ignored an  $\mathcal{O}(|G|^2)$  term so that (8) is valid for perturbations with small  $G$ .

Towards deriving an equation for the numerical computation of  $\nabla \psi_i(\mathbf{x}^\gamma(\theta, \psi_i))$ , we will momentarily take  $G \equiv \mathbf{0}$  and consider the effect of a small perturbation  $\Delta \mathbf{x}$  to a trajectory  $\mathbf{x}(t) \in \gamma$ .  $\Delta \mathbf{x}(t)$

evolves according to

$$\frac{d\Delta\mathbf{x}(t)}{dt} = J(\mathbf{x}(t))\Delta\mathbf{x}(t) + \mathcal{O}(\|\Delta\mathbf{x}\|^2), \quad (9)$$

where  $J(\mathbf{x}(t))$  is the Jacobian matrix evaluated at  $\mathbf{x}(t)$ . The corresponding isostable shift,  $\Delta\psi_i \equiv \psi_i(\mathbf{x}(t) + \Delta\mathbf{x}(t)) - \psi_i(\mathbf{x}(t))$  is given by

$$\Delta\psi_i = \nabla_{\mathbf{x}(t)}\psi_i \cdot \Delta\mathbf{x}(t) + \mathcal{O}(\|\Delta\mathbf{x}\|^2), \quad (10)$$

where  $\nabla_{\mathbf{x}(t)}\psi_i$  is the gradient of  $\psi_i$  evaluated at  $\mathbf{x}(t) \in \gamma$ . After the initial perturbation at  $t = 0$ ,

$$\begin{aligned} \frac{d\Delta\psi_i}{dt} &= \kappa_i \Delta\psi_i \\ &= \kappa_i \nabla_{\mathbf{x}(t)}\psi_i \cdot \Delta\mathbf{x} \end{aligned} \quad (11)$$

In the spirit of [24] and [26], by taking the time derivative of (10) and rearranging, to lowest order in  $\|\Delta\mathbf{x}\|$ ,

$$\begin{aligned} \langle d\nabla_{\mathbf{x}(t)}\psi_i/dt, \Delta\mathbf{x}(t) \rangle &= -\langle \nabla_{\mathbf{x}(t)}\psi_i, d\Delta\mathbf{x}(t)/dt \rangle \\ &\quad + \langle \kappa_i \nabla_{\mathbf{x}(t)}\psi_i, \Delta\mathbf{x} \rangle \\ &= -\langle \nabla_{\mathbf{x}(t)}\psi_i, J(\mathbf{x}(t))\Delta\mathbf{x} \rangle + \langle \kappa_i \nabla_{\mathbf{x}(t)}\psi_i, \Delta\mathbf{x} \rangle \\ &= -\langle J(\mathbf{x}(t))^T \nabla_{\mathbf{x}(t)}\psi_i - \kappa_i \nabla_{\mathbf{x}(t)}\psi_i, \Delta\mathbf{x} \rangle. \end{aligned} \quad (12)$$

Here,  $\langle \cdot, \cdot \rangle$  is the Euclidean inner product (i.e. dot product), and  $^T$  indicates the transpose (i.e. adjoint) of the real-valued matrix  $J(\mathbf{x}(t))$ . Because (12) is valid for any  $\Delta\mathbf{x}$ ,

$$\frac{d\nabla_{\mathbf{x}(t)}\psi_i}{dt} = (\kappa_i I - J(\mathbf{x}(t))^T) \nabla_{\mathbf{x}(t)}\psi_i, \quad (13)$$

where  $I$  is the identity matrix. Note the similarity between (13) and the adjoint equation derived in [21] which was valid only for two-dimensional systems. Recall that for  $\mathbf{x} \in \Gamma_0$ ,  $t_\Gamma = 0$  and  $\mathbf{x}_\Gamma = \mathbf{x}$ , so that from (5),  $\psi_i(\mathbf{x}) = \mathbf{e}_i^T V^{-1}(\mathbf{x} - \mathbf{x}_0)$ . This implies that  $\psi_i(\mathbf{x} + \eta\mathbf{v}_i) = \psi_i(\mathbf{x}) + \eta$  for  $\eta \in \mathbb{R}$ , or equivalently

$$\nabla_{\mathbf{x}_0}\psi_i \cdot \mathbf{v}_i = 1. \quad (14)$$

This normalization condition along with  $T$ -periodicity defines a unique solution of (13). Equation (1) can then be understood in reduced form.

$$\begin{aligned} \dot{\theta} &= \omega + Q^T(\theta) \cdot G(t) \\ \dot{\psi}_i &= \kappa_i \psi_i + \mathcal{I}_i^T(\theta) \cdot G(t) \text{ for } i = 1, \dots, n-1, \end{aligned} \quad (15)$$

where  $Q^T(\theta) \equiv \nabla\theta|_{x^\gamma(\theta)}$  is often referred to as the PRC, and  $\mathcal{I}_i(\theta) \equiv \nabla\psi_i|_{x^\gamma(\theta)}$  will be referred to as an IRC. As shown in Appendix A, the magnitude but not the shape of the resulting IRCs depends on the initial choice of  $\theta(\mathbf{x}_0) = 0$ . Much like in the standard phase reduction (2), the equations (15) are valid provided the unreduced state dynamics remain close to

$\gamma$ . In practice, we generally only need to consider a few isostable coordinates: if  $|\lambda_k| \approx 0$ , any perturbations to  $\psi_k$  will be quickly forgotten and this coordinate can simply be ignored. Finally, we note that if  $J_p$  is not diagonalizable, a similar reduction analysis can be performed for any eigenvalue for which the geometric and algebraic multiplicity are identical. As we will show in the following examples, isostable reduction is essential for understanding phase reduced systems with eigenvalues close to or greater than 1.

To illustrate the principles derived above, we will first consider a three dimensional model of gene regulation [27] which has been used to describe the oscillatory behavior of the suprachiasmatic nucleus responsible for the mammalian circadian clock:

$$\begin{aligned} \dot{X} &= v_1 K_1^n / (K_1^n + Z^n) - v_2 X / (K_2 + X) + L(t), \\ \dot{Y} &= k_3 X - v_4 Y / (K_4 + Y), \\ \dot{Z} &= k_5 Y - v_6 Z / (k_6 + Z). \end{aligned} \quad (16)$$

Here  $X, Y$ , and  $Z$  represent concentrations (expressed in nM) of the mRNA clock gene *per* or *cry*, the PER or CRY protein, and the nuclear form of the protein, respectively with all constants taken as the nominal values from Figure 2 of [27], and  $L(t)$  represents a perturbation from ambient light. Panel (A) of Figure 2 shows the limit cycle solution of (16) when  $L(t) = 0$  with a natural period  $T_c = 23.54$  hours. The value  $\theta = 0$  (an arbitrary reference point) is represented with a black dot, and the  $\Gamma_0$  Poincaré section (i.e., the  $\theta = 0$  isochron) is approximated by the red plane near the periodic orbit. Initial conditions represented by red dots in Panel (D) are mapped to the locations in panel (E). Eigenvalues  $\lambda_1$  and  $\lambda_2$  of eigendirections  $v_1$  and  $v_2$  of  $P(\mathbf{x})$  are determined numerically to be 0.951 and approximately 0, respectively. Using standard techniques [4, 23, 24], the PRC,  $Q^c(\theta) \equiv [Q^X(\theta) Q^Y(\theta) Q^Z(\theta)]$  is calculated with  $Q^X(\theta)$  shown in panel (B). The IRC,  $\mathcal{I}_1^T(\theta) = [\mathcal{I}_1^X(\theta) \mathcal{I}_1^Y(\theta) \mathcal{I}_1^Z(\theta)]$  is calculated using (13) with  $\mathcal{I}_1^X(\theta)$  shown in Panel (C).

We can represent the reduced dynamics of this oscillator with two coupled ordinary differential equations:

$$\dot{\theta} = \omega_c + Q^X(\theta)L(t), \quad (17)$$

$$\dot{\psi}_1 = \kappa_c \psi_1 + \mathcal{I}_1^X(\theta)L(t), \quad (18)$$

with  $\omega_c = 2\pi/T_c$  and  $\kappa_c = \log(\lambda_1)/T_c$ . Note that we do not include  $\psi_2$  in the reduction because the stability in this coordinate is very strong. To illustrate the necessity of (18) in the phase reduction, we will test and implement a simple control strategy for entrainment to an external perturbation. Suppose we would like to entrain the oscillation to an external periodic perturbation  $L(t) = \mu\delta(\text{mod}(t, T_c + \Delta T))$ , a control

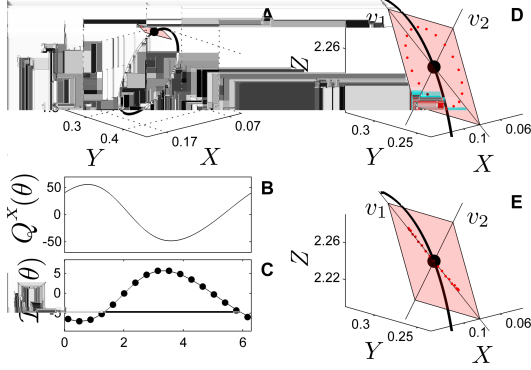


FIG. 2. Panel (A) shows the limit cycle in black with  $\Gamma_0$  in red. Panels (B) and (C) show the PRC and IRC, respectively. Numerical validation of the IRC through calculation of  $\Delta\psi_1/\Delta X$  (represented by black dots) for various phases of perturbation are shown with black dots. Initial conditions (red dots) in panel (D) are mapped to locations in Panel (E) after one iteration of the Poincaré map

objective which is relevant in the treatment in certain types of circadian misalignment (c.f. [28, 29]). By simply taking into account the phase reduction (17), one can understand the phase dynamics as a series of maps

$$\bar{\theta}^+ = \bar{\theta} + 2\pi\Delta T/T_c + \mu Q^X(\bar{\theta}), \quad (19)$$

where  $\bar{\theta}$  represents the phase immediately prior to the application of a pulsatile stimulus, and  $\bar{\theta}^+$  gives the phase at a time  $T_c + \Delta T$  later. Equation (19) has a fixed point when  $\mu = -2\pi\Delta T/T_c Q^X(\bar{\theta})$ . The minimal control effort required occurs when  $\theta = \text{argmax}|Q^X(\theta)| \approx 1$ . Letting  $T_c + \Delta T = 22.2$  hours, simple stability analysis reveals that the resulting fixed point is stable. However, as shown in the right panels of Figure 3 this control strategy does not give stable entrainment and the mean period remains unchanged. From the 3-dimensional trajectory in blue, we find that the trajectory does not remain close to the periodic orbit, as would be predicted from the isostable reduction, as  $\mathcal{I}_1^X(1)$  is relatively large. Instead, if we choose  $\mu$  as above, numerically we find  $\bar{\theta} = 2$  is a stable fixed point of (19), and with  $\mathcal{I}_1^X(1) = 0$ , the pulsatile stimulus stably entrains the oscillator as shown in the left panels of Figure 3. Numerically, we find that fixed points  $\bar{\theta}_0$  of (17) are unstable unless  $\mathcal{I}(\bar{\theta}_0) \approx 0$ .

Next, we show that the notion of isostables can be used to understand the effect of small perturbations near an unstable periodic orbit and how they can be used to optimally drive a given trajectory to an unstable periodic orbit. Here we consider the three

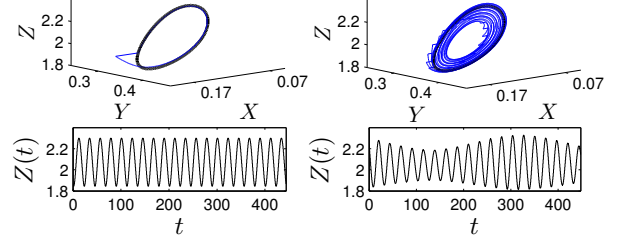


FIG. 3. Left: The circadian oscillator can be entrained (trajectory shown in blue) to periodic  $\delta$ -function perturbations if they are given when the IRC is approximately zero. Right: Entrainment does not occur even when analysis of (17) alone predicts it should. Equation (18) is essential for using phase reduction in this application.

dimensional Lorenz equations [30]:

$$\begin{aligned} \dot{A} &= \sigma(B - A) + u(t), \\ \dot{B} &= A(\rho - C) - B, \\ \dot{C} &= AB - \beta C. \end{aligned} \quad (20)$$

Here,  $A, B$ , and  $C$  are nondimensional system variables,  $\sigma = 16, \beta = 8/3$ , and  $\rho = 350$  are constants chosen so that the unperturbed dynamics are chaotic, and  $u(t)$  is an external perturbation. An unstable periodic orbit,  $\gamma_L$  with period  $T_L = 0.372$  and dynamics along the Lorenz attractor are shown in Figure 4. Along this orbit,  $\theta = 0$  is taken to correspond to an arbitrary location along  $\gamma_L$  allowing for the definition of  $\Gamma_0$ . The resulting Poincaré section is shown in the top-right panel. Eigenvalues  $\lambda_1$  and  $\lambda_2$  of the Poincaré map's  $v_1$  and  $v_2$  eigendirections are numerically determined to be 3.33 and approximately 0, respectively. Using (13) the IRC of this unstable eigendirection  $\mathcal{I}_1^L(\theta) = [\mathcal{I}_1^A(\theta) \mathcal{I}_1^B(\theta) \mathcal{I}_1^C(\theta)]$  is calculated with  $\mathcal{I}_1^A(\theta)$  shown in Figure 5. We also calculate the PRC  $Q^A(\theta)$  for perturbations in the  $A$  direction, allowing for the reduction

$$\begin{aligned} \dot{\theta} &= \omega_L + Q^A(\theta)u(t), \\ \dot{\psi}_1 &= \kappa_L \psi_1 + \mathcal{I}_1^A(\theta)u(t), \end{aligned} \quad (21)$$

where  $\omega_L = 2\pi/T_L$  and  $\kappa_L = \log(\lambda_1)/T_L$ . Understanding the Lorenz system in reduced coordinates allows for the formulation of a control problem to drive any initial condition to the unstable periodic orbit provided it is close enough to the orbit so that the reduction is valid. Towards this calculus of variations problem formulation [31], we define a cost func-

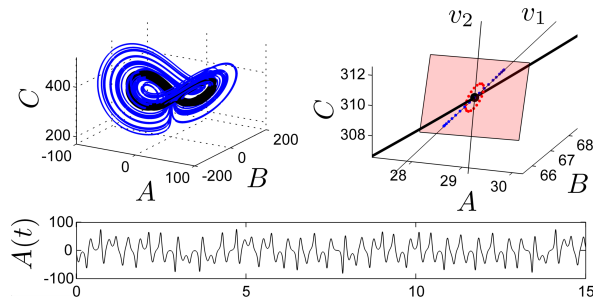


FIG. 4. Top-left: Trajectory along the Lorenz attractor in blue with an unstable periodic orbit outlined in black. Top-right: A small portion of the periodic orbit is shown as a thick black line. Eigendirections of the Poincaré map are shown as thin lines. Initial conditions in red are mapped to the locations in blue after one application of the map. Bottom: an example uncontrolled chaotic trajectory on the Lorenz attractor.

tional

$$\mathcal{M}[\dot{\Phi}, \Phi, u(t)] = \int_0^{T_L} \left[ u^2(t) + \zeta_1 \{ \dot{\theta} - \omega_L - Q^A(\theta)u(t) \} + \zeta_2 \{ \dot{\psi}_1 - \kappa_L \psi_1 - \mathcal{I}_1^A(\theta)u(t) \} \right] dt, \quad (22)$$

with  $\Phi(t) = [\theta(t), \psi_1(t), \zeta_1(t), \zeta_2(t)]$ . Here, Lagrange multipliers  $\zeta_1$  and  $\zeta_2$  force the dynamics to satisfy the phase and isostable reduced equations. The associated Euler-Lagrange equations are

$$\frac{\partial \mathcal{M}}{\partial u} = \frac{d}{dt} \left( \frac{\partial \mathcal{M}}{\partial \dot{u}} \right); \quad \frac{\partial \mathcal{M}}{\partial \Phi} = \frac{d}{dt} \left( \frac{\partial \mathcal{M}}{\partial \dot{\Phi}} \right). \quad (23)$$

Optimal solutions to the cost function satisfy (23) with boundary conditions  $\theta(0) = 0$ ,  $\theta(T_L) = 2\pi$ ,  $\psi_1(T_L) = 0$ , and  $\psi_1(0)$  determined from initial data. This two-point boundary problem can be solved, e.g., with a double bisection algorithm and is chosen so that after one cycle, the trajectory ends on the stable manifold of the Poincaré section  $\Gamma_0$ . The numerically determined optimal control  $u^*(t)$  is shown in Panel (C) of Figure 5 for multiple choices of  $\psi_1(0) \in [-20, 20]$ . In this range,  $u^*(t)$  is approximately proportional to  $1/\psi_1(0)$ . Using this information, we can devise a control algorithm to drive the Lorenz system to the unstable periodic orbit: for any initial condition, wait until the trajectory crosses  $\Gamma_0$  close enough to the unstable periodic orbit, calculate  $\psi_1(0)$  to determine  $u(t)$ . Panels (D) and (E) of Figure 5 show the result of this strategy where the control is set to engage when  $\psi_1(0) < 20$ . After the first control application at  $t \approx 3.5$ , the system is nearly driven to the periodic orbit, but because (13)

provides an approximation to the IRC, a second and third control application (of rapidly decreasing magnitude) are required to bring the system exactly to the periodic orbit.

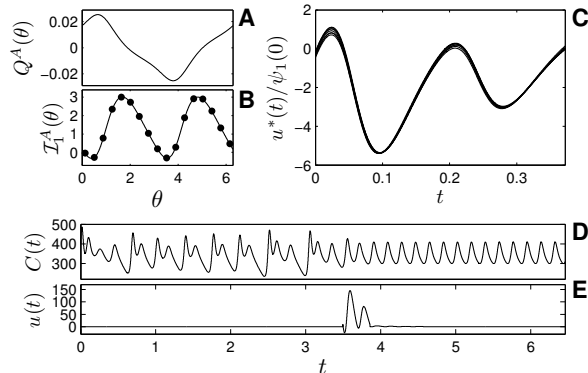


FIG. 5. Panels (A) and (B) give the PRC and IRC for this system. IRC values are numerically validated by calculating  $\Delta\psi_1/\Delta A$  at various phases and shown as black dots. Panel (C) shows an optimal stimulus which takes an initial condition in  $\Gamma_0$  and returns it to  $\Gamma_0$  with  $\psi_1 = 0$  one period later. A control strategy using this information is shown in panels (D) and (E).

The chaos control strategy illustrated here differs from discrete time proportional feedback methods (for example [7], [12]) in that it uses information at all locations near the periodic orbit, not just along the Poincaré surface. This added information about the system allows for the definition of an optimal control problem which yields a continuous solution. In many control applications, allowing for continuous waveforms can lead to a substantial decrease in energy required to achieve a control objective as compared to discrete time control [5], [32]. One drawback of the method developed here is that the periodic orbit must be known before IRCs can be measured and control strategies can be implemented. In this case, in an experimental setting one might envision that the unstable orbit could be found, for instance with delayed feedback control strategies [13], after which an IRC could be measured with an experimental protocol similar to the ‘direct method’ [33], [34] for measuring PRCs. Such a protocol could make a chaos control described here more feasible in an experimental setting.

In summary, we have developed a set of isostable coordinates which allow classical phase reduction to be useful for understanding the dynamics near periodic orbits without Floquet multipliers near 0. The computational complexity of implementing this reduction strategy is comparable to that of standard phase reduction calculations. The reduced dynamics are particularly useful for the problem of stabilizing

unstable periodic orbits as a means of controlling chaotic dynamical systems [7, 12–17]. Additional applications of this reduction strategy could include investigating effect noise on a system in on the dynamics in directions transverse to the periodic orbit (similar to how the variance of the firing rate of an oscillator was studied in [35]). Furthermore, it could be of interest to use this isostable coordinate system to investigate how the phase response characteristics of an oscillator change when perturbed from the periodic orbit, which may have applications to memory effects from pacing history [36], [37]. Continued development of strategies for understanding isostable coordinates of periodic orbits will assist in the understanding of these systems in problems pertaining to synchronization, entrainment, and stabilization of oscillatory dynamics when (2) alone is insufficient.

Support for this work by National Science Foundation Grants NSF-1363243, NSF-1264535, and NSF-1602841 is gratefully acknowledged.

#### Appendix A: Relationship between the choice of Poincaré section and the resulting isostable response curve

In general, the choice of  $\theta = 0$  on the periodic orbit used to define the initial Poincaré section will change the isostable coordinates and will affect resulting isostable response curves. However, the shape of the isostable response curve for any isostable field defined as in (5) from the main text is invariant to the choice of  $\theta$  for which we use to define our Poincaré section provided the algebraic multiplicity of the associated eigenvalue  $\lambda_i$  is unity. This will be shown here by examining the relationship between isostable changes caused by arbitrary perturbations in coordinate systems defined by two different Poincaré sections.

To begin let  $\gamma$  be a  $T$ -periodic solution of the vector field

$$\dot{\mathbf{x}} = F(\mathbf{x}) + G(\mathbf{x}, t), \quad \mathbf{x} \in \mathbb{R}^n \quad (\text{A1})$$

where  $F \in \mathbb{R}^n$  represents the unperturbed dynamics and  $G \in \mathbb{R}^n$  is an external perturbation. As in the main text, we define a scalar phase variable  $\theta(\mathbf{x}) : \mathbb{R}^n \rightarrow [0, 2\pi)$  for which  $d\theta(\mathbf{x}(t))/dt = \omega$  and  $\theta(\mathbf{x}(t)) = \theta(\mathbf{x}(t+T))$ . We also define isochrons to be level sets of the phase field, i.e.  $\Gamma_\theta = \{\mathbf{x} | \theta(\mathbf{x}) = \theta\}$ .

Let  $\mathbf{x}_1$  and  $\mathbf{x}_2$  be any two points on  $\gamma$  such that  $\theta(\mathbf{x}_1) = \theta_1$  and  $\theta(\mathbf{x}_2) = \theta_2$ . The associated isochrons,  $\Gamma_{\theta_1}$  and  $\Gamma_{\theta_2}$  can be used to define Poincaré

maps

$$P_1 : \Gamma_{\theta_1} \rightarrow \Gamma_{\theta_1} \\ \mathbf{x} \mapsto \phi_1(\mathbf{x}), \quad (\text{A2})$$

$$P_2 : \Gamma_{\theta_2} \rightarrow \Gamma_{\theta_2} \\ \mathbf{x} \mapsto \phi_2(\mathbf{x}). \quad (\text{A3})$$

In the analysis to follow, we will restrict our attention to the dynamics of these maps in a small neighborhood of  $\mathbf{x}_1$  and  $\mathbf{x}_2$ . Taylor expanding, one can show that for any time  $t_1$  (resp.  $t_2$ ) for which  $\mathbf{x}(t_1) \in \Gamma_{\theta_1}$  (resp.  $\mathbf{x}(t_2) \in \Gamma_{\theta_2}$ ),

$$\mathbf{x}(T + t_1) - \mathbf{x}_1 = J_1(\mathbf{x}(t_1) - \mathbf{x}_1) + \mathcal{O}(\|\mathbf{x}(t_1) - \mathbf{x}_1\|^2), \\ \mathbf{x}(T + t_2) - \mathbf{x}_2 = J_2(\mathbf{x}(t_2) - \mathbf{x}_2) + \mathcal{O}(\|\mathbf{x}(t_2) - \mathbf{x}_2\|^2), \quad (\text{A4})$$

where  $J_1 = d\phi_1/d\mathbf{x}|_{\mathbf{x}_1}$  and  $J_2 = d\phi_2/d\mathbf{x}|_{\mathbf{x}_2}$ . By construction of the phase field,  $\Gamma_{\theta_2}$  is the image of  $\Gamma_{\theta_1}$  under the flow of the vector field (A1) with  $G \equiv 0$ . As discussed in Chapter 11 of [38], this defines a  $C^r$  diffeomorphism

$$h : \Gamma_{\theta_1} \rightarrow \Gamma_{\theta_2} \\ \mathbf{x} \mapsto \xi(\mathbf{x}) \quad (\text{A5})$$

and implies that the eigenvalues of  $J_1$  are equal to the eigenvalues of  $J_2$ . Note that  $h(\mathbf{x}_1) = \mathbf{x}_2$  so that in a small neighborhood of  $\mathbf{x}_1$ , we can approximate (A5) as

$$h(\mathbf{x}) = \mathbf{x}_2 + H(\mathbf{x} - \mathbf{x}_1) + \mathcal{O}(\|\mathbf{x} - \mathbf{x}_1\|^2), \quad (\text{A6})$$

where  $H = d\xi/d\mathbf{x}|_{\mathbf{x}_1}$

Towards the definition of isostables with respect to each map, suppose the  $J_1$  and  $J_2$  are both diagonalizable. Let  $V_1$  (resp.  $V_2$ )  $\in \mathbb{R}^{n \times n}$  be matrices with columns that form an orthonormal basis of unit length eigenvectors  $\{\mathbf{v}_k^1, k = 1, \dots, n\}$  of  $J_1$  (resp.  $\{\mathbf{v}_k^2, k = 1, \dots, n\}$  of  $J_2$ ) associated with the eigenvalues  $\{\lambda_k, k = 1, \dots, n\}$ .

Let  $\mathbf{e}_i$  be a vector with 1 in the  $i^{\text{th}}$  position and zeros elsewhere. Mirroring the definition used in the main text, we define two isostable fields  $\psi_i^1$  and  $\psi_i^2$  with respect to the Poincaré sections  $\Gamma_{\theta_1}$  and  $\Gamma_{\theta_2}$ :

$$\psi_i^j(\mathbf{x}) = \mathbf{e}_i^T V_j^{-1}(\mathbf{x}_{\Gamma_j} - \mathbf{x}_j) \exp(-\log(\lambda_i)t_{\Gamma_j}/T), \\ j = 1, 2, \quad (\text{A7})$$

where  $\mathbf{x}_{\Gamma_1}$  and  $t_{\Gamma_1}$  (resp.  $\mathbf{x}_{\Gamma_2}$  and  $t_{\Gamma_2}$ ) are the location and time, respectively, at which the trajectory under the flow  $\dot{\mathbf{x}} = F(\mathbf{x})$  next returns to  $\Gamma_{\theta_1}$  (resp.  $\Gamma_{\theta_2}$ ). Here,  $^{-1}$  denotes the matrix inverse and  $^T$  denotes the matrix transpose. To present the following derivation in a more intuitive way, we will define the scalars  $s_i^1(\mathbf{x}) \equiv \mathbf{e}_i^T V_1^{-1}\mathbf{x}$  and  $s_i^2(\mathbf{x}) \equiv \mathbf{e}_i^T V_2^{-1}\mathbf{x}$

which give the coordinates of  $\mathbf{x}$  in the basis of eigenvectors of  $J_1$  and  $J_2$ , respectively. Using (A4), one can show that

$$\begin{aligned} s_i^1(\mathbf{x}(T+t_1) - \mathbf{x}_1) &= \lambda_i s_i^1(\mathbf{x}(t_1) - \mathbf{x}_1) \\ s_i^2(\mathbf{x}(T+t_2) - \mathbf{x}_2) &= \lambda_i s_i^2(\mathbf{x}(t_2) - \mathbf{x}_2). \end{aligned} \quad (\text{A8})$$

For convenience of notation in (A8) we have dropped the higher order error terms that would carry through from (A4).

Consider any initial condition  $\mathbf{x}(0) \in \Gamma_{\theta_1}$ . Written in the basis of eigenvectors of  $J_1$

$$\begin{aligned} \mathbf{x}(0) - \mathbf{x}_1 &= s_1^1(\mathbf{x}(0) - \mathbf{x}_1)v_1^1 \\ &\quad + \cdots + s_n^1(\mathbf{x}(0) - \mathbf{x}_1)v_n^1 \\ \mathbf{x}(T) - \mathbf{x}_1 &= \lambda_1 s_1^1(\mathbf{x}(0) - \mathbf{x}_1)v_1^1 \\ &\quad + \cdots + \lambda_n s_n^1(\mathbf{x}(0) - \mathbf{x}_1)v_n^1, \end{aligned} \quad (\text{A9})$$

where we have used (A8) to obtain the second line. Using (A6), we can write to leading order  $\|\mathbf{x}(0) - \mathbf{x}_1\|^2$ ,

$$\begin{aligned} \mathbf{x}(\Delta t) - \mathbf{x}_2 &= H[s_1^1(\mathbf{x}(0) - \mathbf{x}_1)v_1^1 \\ &\quad + \cdots + s_n^1(\mathbf{x}(0) - \mathbf{x}_1)v_n^1] \\ \mathbf{x}(\Delta t + T) - \mathbf{x}_2 &= H[\lambda_1 s_1^1(\mathbf{x}(0) - \mathbf{x}_1)v_1^1 \\ &\quad + \cdots + \lambda_n s_n^1(\mathbf{x}(0) - \mathbf{x}_1)v_n^1]. \end{aligned} \quad (\text{A10})$$

Here  $\Delta t = \omega(\theta_2 - \theta_1)$  with  $\dot{\theta} = \omega$  under the flow  $\dot{\mathbf{x}} = F(\mathbf{x})$ . When calculating isostables using (A7)  $t_{\Gamma_2} = 0$  for any  $\mathbf{x} \in \Gamma_{\theta_2}$ . Because  $\mathbf{x}(\Delta t) \in \Gamma_{\theta_2}$ ,  $\psi_i^2(\mathbf{x}(\Delta t)) = s_i^2(\mathbf{x}(\Delta t) - \mathbf{x}_2)$ . Also,  $\mathbf{x}(\Delta t + T) \in \Gamma_{\theta_2}$ , and using (A8),  $\psi_i^2(\mathbf{x}(\Delta t + T)) = \lambda_i s_i^2(\mathbf{x}(\Delta t) - \mathbf{x}_2)$ . With (A10), this implies

$$\begin{aligned} \lambda_i s_i^2(H[s_1^1(\mathbf{x}(0) - \mathbf{x}_1)v_1^1 + \cdots + s_n^1(\mathbf{x}(0) - \mathbf{x}_1)v_n^1]) \\ = s_i^2(H[\lambda_1 s_1^1(\mathbf{x}(0) - \mathbf{x}_1)v_1^1 \\ + \cdots + \lambda_n s_n^1(\mathbf{x}(0) - \mathbf{x}_1)v_n^1]). \end{aligned} \quad (\text{A11})$$

Equation (A11) holds for any  $\mathbf{x}(0)$ . We will assume that  $\lambda_i$  has an algebraic multiplicity of 1 so that by linearity of  $s_i^1$  and  $s_i^2$ , (A11) implies

$$s_i^2(Hv_j^1) = 0 \text{ for all } j \neq i, \quad (\text{A12})$$

and

$$s_i^2(H(\mathbf{x} - \mathbf{x}_1)) = s_i^1(\mathbf{x} - \mathbf{x}_1)s_i^2(Hv_i^1). \quad (\text{A13})$$

Using this information, we can now show that the isostable response curve is invariant to the value of  $\theta$  we use for our initial Poincaré section.

Consider any initial condition  $\mathbf{z}(0) \in \mathbb{R}^n$  which returns to  $\Gamma_{\theta_1}$  at time  $t_1$ . Let  $s_i^1(\mathbf{z}(t_1) - \mathbf{x}_1) = \beta$ , then by (A7)

$$\psi_i^1(\mathbf{z}(0) - \mathbf{x}_1) = \beta \exp(-\log(\lambda_i)t_1/T). \quad (\text{A14})$$

Now consider a perturbed initial condition  $\mathbf{y}(0) = \mathbf{z}(0) + \Delta \mathbf{x}$  which returns to  $\Gamma_{\theta_1}$  at time  $t_1 + p$  with  $s_i^1(\mathbf{y}(t_1 + p) - \mathbf{x}_1) = \mu + \beta$ . We can write

$$\psi_i^1(\mathbf{y}(0) - \mathbf{x}_1) = (\mu + \beta) \exp(-\log(\lambda_i)(t_1 + p)/T) \quad (\text{A15})$$

so that

$$\begin{aligned} \psi_i^1(\mathbf{y}(0) - \mathbf{x}_1) - \psi_i^1(\mathbf{z}(0) - \mathbf{x}_1) &= \\ &= (\mu + \beta) \exp(-\log(\lambda_i)(t_1 + p)/T) \\ &\quad - \beta \exp(-\log(\lambda_i)t_1/T) \\ &\equiv \Lambda. \end{aligned} \quad (\text{A16})$$

Now consider the isostables with respect to the  $\Gamma_{\theta_2}$  Poincaré section. Each trajectory will reach  $\Gamma_{\theta_2}$  at a time  $\Delta t$  after it reaches  $\Gamma_{\theta_1}$ . Using (A6),

$$\begin{aligned} \mathbf{z}(t_1 + \Delta t) &= H(\mathbf{z}(t_1) - \mathbf{x}_1) + \mathbf{x}_2 \\ &\quad + \mathcal{O}(\|\mathbf{z}(t_1) - \mathbf{x}_1\|^2) \\ \mathbf{y}(t_1 + p + \Delta t) &= H(\mathbf{y}(t_1 + p) - \mathbf{x}_1) + \mathbf{x}_2 \\ &\quad + \mathcal{O}(\|\mathbf{y}(t_1 + p) - \mathbf{x}_1\|^2). \end{aligned} \quad (\text{A17})$$

Using (A13), we find

$$\begin{aligned} \psi_i^2(\mathbf{z}(0) - \mathbf{x}_2) &= \beta s_i^2(Hv_i^1) \\ &\quad \times \exp(-\log(\lambda_i)(t_1 + \Delta t)/T) \\ \psi_i^2(\mathbf{y}(0) - \mathbf{x}_2) &= (\mu + \beta) s_i^2(Hv_i^1) \\ &\quad \times \exp(-\log(\lambda_i)(t_1 + p + \Delta t)/T). \end{aligned} \quad (\text{A18})$$

Algebraic manipulation yields

$$\begin{aligned} \psi_i^2(\mathbf{y}(0) - \mathbf{x}_2) - \psi_i^2(\mathbf{z}(0) - \mathbf{x}_2) \\ = s_i^2(Hv_i^1) \exp(-\log(\lambda_i)\Delta t/T) \Lambda. \end{aligned} \quad (\text{A19})$$

Note here that  $s_i^2(Hv_i^1)$  and  $\exp(-\log(\lambda_i)\Delta t/T)$  are both constant terms so that equations (A16) and (A19) imply that regardless of which isochron is chosen for the Poincaré section to define isostables, the shape of the resulting isostable response curves will be identical provided  $\lambda_i$  has an algebraic multiplicity of 1. The magnitude of the isostable response curve can vary depending on the geometry of the periodic orbit.



- 
- [1] A. T. Winfree. Patterns of phase compromise in biological cycles. *Journal of Mathematical Biology*, 1(1):73–93, 1974.
- [2] J. Guckenheimer. Isochrons and phaseless sets. *Journal of Mathematical Biology*, 1(3):259–273, 1975.
- [3] Y. Kuramoto. *Chemical Oscillations, Waves, and Turbulence*. Springer-Verlag, Berlin, 1984.
- [4] F. C. Hoppensteadt and E. M. Izhikevich. *Weakly Connected Neural Networks*. Springer, 1997.
- [5] D. Wilson and J. Moehlis. Optimal chaotic desynchronization for neural populations. *SIAM Journal on Applied Dynamical Systems*, 13(1):276–305, 2014.
- [6] D. Wilson and J. Moehlis. Clustered desynchronization from high-frequency deep brain stimulation. *PLoS Comput. Biol.*, 11(12):e1004673, 2015.
- [7] E. Ott, C. Grebogi, and J. A. Yorke. Controlling chaos. *Physical Review Letters*, 64(11):1196, 1990.
- [8] J. Guckenheimer and P. Holmes. *Nonlinear Oscillations, Dynamical Systems, and Bifurcations of Vector Fields*, volume 42. Springer Verlag, New York, 1983.
- [9] A. Zlotnik, Y. Chen, I. Z. Kiss, H. A. Tanaka, and J. S. Li. Optimal waveform for fast entrainment of weakly forced nonlinear oscillators. *Physical Review Letters*, 111(2):024102, 2013.
- [10] R. Snari and M. R. Tinsley, D. Wilson, S. Faramarzi, T. I. Netoff, J. Moehlis, and K. Showalter. Desynchronization of stochastically synchronized chemical oscillators. *Chaos*, 25(12):123116, 2015.
- [11] I. Z. Kiss, C. G. Rusin, H. Kori, and J. L. Hudson. Engineering complex dynamical structures: sequential patterns and desynchronization. *Science*, 316:1886–1889, 2007.
- [12] F. J. Romeiras, C. Grebogi, E. Ott, and W. P. Dayawansa. Controlling chaotic dynamical systems. *Physica D*, 58(1-4):165–192, 1992.
- [13] K. Pyragas. Continuous control of chaos by self-controlling feedback. *Physics letters A*, 170(6):421–428, 1992.
- [14] D. J. Christini, M. L. Riccio, C. A. Culianu, J. J. Fox, A. Karma, and R. F. Gilmour Jr. Control of electrical alternans in canine cardiac Purkinje fibers. *Physical Review Letters*, 96(10):104101, 2006.
- [15] R. Meucci, S. Euzzor, E. Pugliese, S. Zambrano, M. R. Gallas, and J. A. C. Gallas. Optimal phase-control strategy for damped-driven Duffing oscillators. *Physical Review Letters*, 116(4):044101, 2016.
- [16] J. Sieber, E. Omelchenko, and M. Wolfrum. Controlling unstable chaos: stabilizing chimera states by feedback. *Physical Review Letters*, 112(5):054102, 2014.
- [17] W. Lu, E. Yu, and R. G. Harrison. Control of patterns in spatiotemporal chaos in optics. *Physical Review Letters*, 76(18):3316, 1996.
- [18] A. Mauroy, I. Mezić, and J. Moehlis. Isostables, isochrons, and Koopman spectrum for the action-angle representation of stable fixed point dynamics. *Physica D: Nonlinear Phenomena*, 261:19–30, 2013.
- [19] A. J. Roberts. Appropriate initial conditions for asymptotic descriptions of the long term evolution of dynamical systems. *The Journal of the Australian Mathematical Society. Series B. Applied Mathematics*, 31(01):48–75, 1989.
- [20] S. M. Cox and A. J. Roberts. Initial conditions for models of dynamical systems. *Physica D: Nonlinear Phenomena*, 85(1):126–141, 1995.
- [21] O. Castejón, A. Guillamon, and G. Huguet. Phase-amplitude response functions for transient-state stimuli. *J. Math. Neurosci.*, 3:13, 2013.
- [22] A. Guillamon and G. Huguet. A computational and geometric approach to phase resetting curves and surfaces. *SIAM Journal on Applied Dynamical Systems*, 8(3):1005–1042, 2009.
- [23] G. B. Ermentrout and N. Kopell. Multiple pulse interactions and averaging in systems of coupled neural oscillators. *Journal of Mathematical Biology*, 29(3):195–217, 1991.
- [24] E. Brown, J. Moehlis, and P. Holmes. On the phase reduction and response dynamics of neural oscillator populations. *Neural Computation*, 16(4):673–715, 2004.
- [25] Y. Kuramoto. Phase-and center-manifold reductions for large populations of coupled oscillators with application to non-locally coupled systems. *International Journal of Bifurcation and Chaos*, 7(04):789–805, 1997.
- [26] D. Wilson and J. Moehlis. Extending phase reduction to excitable media: Theory and applications. *SIAM Review*, 57(2):201–222, 2015.
- [27] D. Gonze, S. Bernard, C. Waltermann, A. Kramer, and H. Herzel. Spontaneous synchronization of coupled circadian oscillators. *Biophysical Journal*, 89(1):120–129, 2005.
- [28] D. Wilson and J. Moehlis. An energy-optimal approach for entrainment of uncertain circadian oscillators. *Biophysical Journal*, 107(7):1744–1755, 2014.
- [29] Y. Xu, Q. S. Padiath, R. E. Shapiro, C. R. Jones, S. C. Wu, N. Saigoh, K. Saigoh, L. J. Ptáček, and Fu Y. H. Functional consequences of a CK1 $\delta$  mutation causing familial advanced sleep phase syndrome. *Nature*, 434(7033):640–644, 2005.
- [30] E. N. Lorenz. Deterministic nonperiodic flow. *Journal of the Atmospheric Sciences*, 20(2):130–141, 1963.
- [31] D. Kirk. *Optimal Control Theory*. Dover Publications, New York, 1998.
- [32] A. Nabi, T. Stigen, J. Moehlis, and T. Netoff. Minimum energy control for *in vitro* neurons. *Journal of Neural Engineering*, 10(3):036005, 2013.
- [33] E. M. Izhikevich. *Dynamical Systems in Neuroscience: The Geometry of Excitability and Bursting*. MIT Press, London, 2007.
- [34] T. Netoff, M. A. Schwemmer, and T. J. Lewis. Experimentally estimating phase response curves of neurons: theoretical and practical issues. In *Phase Response Curves in Neuroscience*, pages 95–129.

- Springer, 2012.
- [35] G. B. Ermentrout, B. Beverlin II, T. Troyer, and T. I. Netoff. The variance of phase-resetting curves. *Journal of Computational Neuroscience*, 31(2):185–197, 2011.
- [36] S. K. Maran and C. C. Canavier. Using phase resetting to predict 1:1 and 2:2 locking in two neuron networks in which firing order is not always preserved. *Journal of Computational Neuroscience*, 24(1):37–55, 2008.
- [37] J. Cui, C. C. Canavier, and R. J. Butera. Functional phase response curves: A method for understanding synchronization of adapting neurons. *Journal of Neurophysiology*, 102(1):387–398, 2009.
- [38] S. Wiggins. *Introduction to Applied Nonlinear Dynamical Systems and Chaos*, volume 2. Springer, 2003.